Journal of Solid State Chemistry **165,** 261–265 (2002)
doi:10.1006/jssc.2002.9519, available online at http://www/idealibrary.com on IDEAL®

The Synthesis and Crystal Structure of Doped Uranium Brannerite Phases $U_{1-x}M_xTi_2O_6$ (M=Ca^{2+}, La^{3+}, and Gd^{3+})

M. James*,[1] and J. N. Watson†

*Neutron Scattering Group; and †Materials Division, Australian Nuclear Science and Technology Organisation, PMB 1, Menai NSW 2234, Australia

Received October 8, 2001; in revised form January 17, 2002; accepted January 25, 2002; published online March 22, 2002

Doped uranium brannerite phases ($U_{1-x}M_xTi_2O_6$; $M = Ca^{2+}$, La^{3+} and Gd^{3+}; $x < 0.5$) were synthesized at 1400°C; the range of solid solution was found to vary depending on whether sintering took place in argon or air. Powder X-ray diffraction revealed that these phases crystallized to form monoclinic ($C2/m$) structures. In particular, the crystal structures of $U_{0.74}Ca_{0.26}Ti_2O_6$ (1) ($a = 9.8008(2)$; $b = 3.7276(1)$; $c = 6.8745(1)$; $\beta = 118.38(1)$; $V = 220.97(1)$; $Z = 2$; $R_P = 7.3\%$; $R_B = 4.6\%$) and $U_{0.55}La_{0.45}Ti_2O_6$ (2) ($a = 9.8002(7)$; $b = 3.7510(3)$; $c = 6.9990(5)$; $\beta = 118.37(4)$; $V = 226.40(3)$; $Z = 2$; $R_P = 4.5\%$; $R_B = 2.9\%$) were refined from powder neutron diffraction data, revealing planes of corner and edge-sharing TiO_6 octahedra separated by 8-fold coordinate U/M atoms. The oxygen sites within these structures were found to be fully occupied, confirming that the doping of lower valence M atoms occurs in conjunction with the oxidation of U(IV) to U(V).

Key Words: **doped uranium brannerite; powder neutron diffraction; Rietveld refinement; nuclear waste immobilization.**

INTRODUCTION

Brannerite, UTi_2O_6, occurs as a mineral that is nearly always X-ray amorphous because of radiation damage from α-decay of U, Th and daughter isotopes. It can, however, be recrystallized by heating to temperatures of approximately 1000°C and leads to a monoclinic crystal structure (1, 2). It is a minor phase in titanate-based pyrochlore-rich ceramics of the Synroc (3) type designed for the geological immobilization of excess weapons Pu (4, 5). Brannerite in the ceramics was found to incorporate Pu together with neutron absorbers such as Gd and Hf as well as Pu and U. The neutron absorbers serve to overcome potential criticality problems associated with the presence of Pu. Recent examination of the kinetics of uranium release from a number of titanate-based Synroc phases revealed that pyrochlore and zirconolite ceramics demonstrated higher chemical durability and more resistance to aqueous attack than brannerite (6). The presence of brannerite inclusions in pyrochlore-rich ceramics, however, did not appear to have a detrimental effect on uranium release.

As pure UTi_2O_6 can only be synthesized by dry ceramic techniques under low-oxygen conditions (1), it is clear that incorporation of other impurity ions provides a means of stabilizing brannerite phases produced in air. In a recent study, we reported the formation of $U_{1-x}M_xTi_2O_6$ brannerite phases in both air and argon for a wide range of ionic substituents ($M = Ca^{2+}$, La^{3+}, Gd^{3+}, Y^{3+}, Hf^{4+} and Pu^{4+}) (7).

The present work investigates the substitutional chemistry of brannerite phases $U_{1-x}M_xTi_2O_6$ ($M = Ca^{2+}$, La^{3+} and Gd^{3+}; $x < 0.5$), in relation to the crystal structures of these compounds. In particular, we report the structures of $U_{0.74}Ca_{0.26}Ti_2O_6$ (1), $U_{0.55}La_{0.45}Ti_2O_6$ (**2**) as determined by powder neutron diffraction.

EXPERIMENTAL

Synthesis

The samples were prepared by the alkoxide/nitrate route (8); the mixtures were dried and then calcined in either air or argon (containing < 10 ppm O_2) at 750°C for 1 h. The calcines were wet milled for 16 h and dried before cold pressing and firing the pellets for 14 h at 1400°C under air or argon and furnace cooled at a rate of 5°C/min.

Electron Microscopy

Scanning electron microscopy (SEM) was carried out with a JEOL 6400 instrument run at 15 kV, and fitted with a Tracor Northern TN5502 energy-dispersive X-ray fluorescence analyser, which utilized a comprehensive set of standards for quantitative work.

[1]To whom correspondence should be addressed. Fax: +61-2-9717-3606. E-mail: mja@ansto.gov.au.

0022-4596/02 $35.00

Diffraction Measurements

Powder X-ray diffraction measurements were made on a Scintag Inc. XGEN 4000 X-ray diffractometer at ambient temperature using Cu$K\alpha$ radiation and a flat-plate sample holder. Data of sufficient quality for structural refinement were collected over $5^\circ < 2\Theta < 85^\circ$, in 0.025° steps, with integration times of 10 s. Powder neutron diffraction measurements were also made on the medium- and high-resolution powder diffractometers using thermal neutrons [$\lambda = 1.6653$ Å (MRPD), ($\lambda = 1.8855$ Å (HRPD)] from the HIFAR nuclear reactor at ANSTO (9). Data were collected using a bank of 32 ^{3}He detectors over the range $-4^\circ < 2\Theta < 138^\circ$, in 0.1° steps (MRPD) or 24 ^{3}He detectors over the range $0^\circ < 2\Theta < 153^\circ$, in 0.05° steps (HRPD). Structural refinements were carried out by the Rietveld method (10) using the RIETICA program, (11) with Voigt peak shapes and refined backgrounds.

RESULTS AND DISCUSSION

Solid Solution Range

Our previous work indicated that sintering the correct stoichiometry in argon produced single-phase brannerite UTi_2O_6, whereas sintering in air produced U_3O_8 and TiO_2. Brannerite phases were stabilized in an air atmosphere at high temperatures by substitution of Ca^{2+}, La^{3+} or Gd^{3+} for U^{4+}. Diffuse reflectance spectroscopy revealed the presence of U^{5+} ions, which suggested that stabilization of these doped phases was via a charge compensation mechanism rather than the formation of oxygen vacancies (7). No evidence of green fluorescence characteristic of U^{6+} was observed.

In the present work, the solid solution ranges for the phases $U_{1-x}M_xTi_2O_6$ ($M = Ca^{2+}$, La^{3+} and Gd^{3+}) were found to vary with the oxidation state of the dopant and the atmosphere. Under-doped samples prepared in air gave rise to brannerite phases, U_3O_8 and TiO_2 impurities, while over-doped samples contained brannerite phases, TiO_2 and pyrochlore phases ($M_{1+x}U_{1-x}Ti_2O_7$). Scanning electron microscopy was used to characterize the solid solution ranges for the $U_{1-x}M_xTi_2O_6$ phases formed at 1400°C; the results of which are given in Table 1. In general terms, it may be seen that sintering these phases in argon leads to a wider solid solution range than for those sintered in air. In addition, sintering in air allows access to higher doping levels than observed for sintering under argon. Given the assumptions that no oxygen vacancies are produced and that U(IV) is oxidized to U(V) in order to compensate for the introduction of dopants with lower oxidation states, we can determine the relative levels of U(IV) and U(V) in these phases. Under argon between 0 and 50% U(V) is present in the phases $U_{1-x}Ca_xTi_2O_6$, while sintering in air gives rise to between 53 and 78% U(V). In the case of the lanthanide-doped brannerite phases, argon sintering allows for between 0 and 82% U(V), whereas samples sintered in air gave rise to between 45 and 100% U(V). As the above results indicate, almost as much Ca, La or Gd can be substituted into the brannerite structure under a neutral atmosphere such as argon, as can be achieved under an oxidizing atmosphere such as air. This demonstrates the important role that the crystal chemistry plays in the solid solubility, as well as the oxygen pressure in the firing atmosphere.

TABLE 1
Solid Solution Ranges for $U_{1-x}M_xTi_2O_6$ Phases Prepared at 1400°C in Air or Argon

$U_{1-x}M_xTi_2O_6$	Prepared in air (1400°C)	Prepared in argon (1400°C)
Ca^{2+}	$0.21 \le x \le 0.28$	$0 \le x \le 0.20$
La^{3+}	$0.38 \le x \le 0.50$	$0 \le x \le 0.45$
Gd^{3+}	$0.31 \le x \le 0.50$	$0 \le x \le 0.45$

Structural Refinements

X-ray diffraction profiles. Figure 1 shows the X-ray diffraction profiles of $U_{0.74}Ca_{0.26}Ti_2O_6$ (**1**) which is typical of those observed for $U_{1-x}M_xTi_2O_6$ ($M = Ca^{2+}$, La^{3+}, and Gd^{3+}). In each case, these diffraction patterns could be indexed based on the known monoclinic $C2/m$ cell of uranium brannerite UTi_2O_6 (1). Attempts to refine the structures of these phases using the structure of UTi_2O_6 as an initial model were, however, totally unsuccessful, leading to very high residuals ($R_p \sim 40\%$) or unstable refinements. Comparison of the observed diffraction

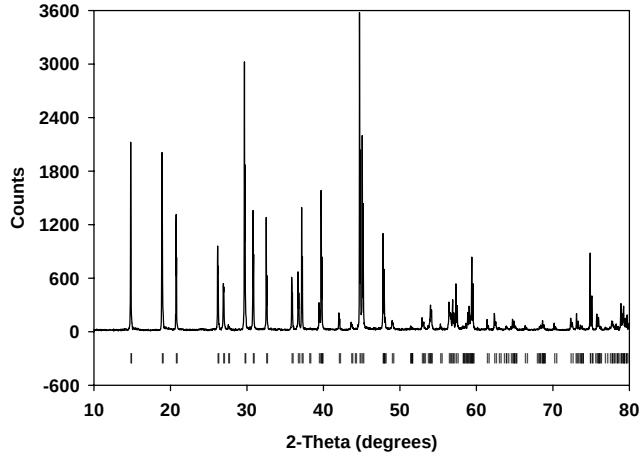

FIG. 1. The observed powder X-ray diffraction profile for $U_{0.74}Ca_{0.26}Ti_2O_6$ (**1**).

TABLE 2
Lattice Parameters of $U_{1-x}M_xTi_2O_6$ Phases Synthesized at 1400°C as Determined from Powder XRD Data

X	a (Å)	b (Å)	c (Å)	β (°)	V (Å^3)
Synthesized in air					
$U_{1-x}Ca_xTi_2O_6$					
0.21	9.796(3)	3.727(1)	6.879(2)	118.42(1)	220.9(1)
0.28	9.795(3)	3.724(1)	6.871(2)	118.23(1)	220.8(1)
$U_{1-x}La_xTi_2O_6$					
0.38	9.798(2)	3.752(1)	6.984(2)	118.36(1)	225.9(1)
0.50	9.809(2)	3.749(1)	7.007(1)	118.31(1)	226.9(1)
$U_{1-x}Gd_xTi_2O_6$					
0.31	9.808(1)	3.736(1)	6.891(1)	118.56(1)	221.8(1)
0.50	9.815(1)	3.729(1)	6.889(1)	118.55(1)	221.5(1)
Synthesized in Ar					
$U_{1-x}Ca_xTi_2O_6$					
0[a]	9.812(2)	3.770(1)	6.925(1)	119.0(1)	224.1(1)
0.20	9.810(1)	3.739(1)	6.897(1)	118.57(1)	222.2(1)
$U_{1-x}La_xTi_2O_6$					
0[a]	9.812(2)	3.770(1)	6.925(1)	119.0(1)	224.1(1)
0.45	9.903(1)	3.747(1)	6.995(1)	118.32(1)	226.2(1)
$U_{1-x}Gd_xTi_2O_6$					
0[a]	9.812(2)	3.770(1)	6.925(1)	119.0(1)	224.1(1)
0.45	9.819(2)	3.742(1)	6.905(1)	118.71(1)	222.6(1)

[a]Taken from Ref. (1).

profiles with those calculated from idealized structures based on UTi_2O_6 indicated strong preferred orientation of the crystallites. Refinement of the Dollase preferred orientation function (12) along different directions did not lead to significant improvements in the fit to the data. Examination of the refined structures revealed significant "non-physical" distortions, serving to highlight the difficulty in modelling substantial preferred orientation when using flat-plate Bragg–Brentano powder X-ray diffraction data.

Unit cell parameters were, however, able to be extracted from the powder X-ray diffraction data using the RIETICA program and the Le Bail method (13). Table 2 contains cell parameters extracted from powder XRD data for end-member compositions that were formed in either air or argon. Examination of Table 2 reveals the effect of doping on the brannerite structure. The replacement of U^{4+} having an ionic radius of 1.00 Å (14) by the larger Ca^{2+} ion (1.12 Å) is off-set by the oxidation of 78% of the remaining uranium to the smaller (0.86 Å) U^{5+}. The doping and corresponding oxidation of some of the U(IV) lead to a contraction in the unit cell size from 224.1(1) Å for UTi_2O_6 (1) to 220.8(1) Å in $U_{0.72}Ca_{0.28}Ti_2O_6$. Due to the difference in valency between Ca^{2+} and U^{4+}, there are of course two smaller U^{5+} ions produced for every Ca^{2+} introduced into the structure. In the case of $U_{0.5}La_{0.5}Ti_2O_6$ all of the uranium was oxidized to U^{5+}; however, the larger La^{3+} ions (1.16 Å) led to an increase in the size of this unit cell [226.9(1) Å]. Here, only one U^{5+} ion was required per introduced La^{3+} in order to maintain charge neutrality.

Neutron diffraction profiles. Due to the difference in scattering geometry, preferred orientation concerns were removed from the structural refinements when powder neutron diffraction data were used. Neutron diffraction data have the additional benefit of providing increased contrast with respect to the oxygen atoms than could be obtained by XRD, particularly given the presence of heavy atoms such as calcium, lanthanum and uranium. Gadolinium being a strong neutron absorber (with an absorption cross-section $\sigma_a = 49{,}700$ barn for 2200 ms^{-1} neutrons) meant that neutron diffraction data could not be collected for Gd-containing samples. In these cases, structural conclusions may be drawn from the La-doped phases with a substantially smaller neutron adsorption cross-section ($\sigma_a = 8.97$ barn). Refinement of the structures of these latter samples, however, was complicated by the fact that U and La have almost identical neutron scattering factors ($b = 0.85 \times 10^{-12}$ cm and 0.83×10^{-12} cm, respectively).

The structural parameters for **1** and **2** were determined by Rietveld refinement using the RIETICA program in space group $C2/m$ with M and U disordered over the actinide $2a$ (0,0,0) sites (Table 3). As the diffraction profiles for **1** and **2** revealed phase pure samples the occupancies of Ca, La and U in their respective compounds were set at their nominal compositions. In the final stages of the refinement the oxygen sites of **1** and **2** were refined and were found to be fully occupied, this being consistent with the oxidation of U(IV) to U(V) and no formation of oxygen vacancies. The observed, calculated and difference diffraction profiles for **1** and **2** are shown in Fig. 2, while

TABLE 3
Crystallographic Data for $U_{0.74}Ca_{0.26}Ti_2O_6$ (1) and $U_{0.55}La_{0.45}Ti_2O_6$ (2) as Determined from Powder Neutron Diffraction Data

	1	**2**
Formula	$U_{0.74}Ca_{0.26}Ti_2O_6$	$U_{0.55}La_{0.45}Ti_2O_6$
Formula weight	363.806	384.290
U^{4+}; U^{5+} (%)	30; 70	18; 82
Space group	$C2/m$ (No. 12)	$C2/m$
Z	2	2
a (Å)	9.8008(2)	9.8002(7)
b (Å)	3.7276(1)	3.7510(3)
c (Å)	6.8745(1)	6.9990(5)
β (°)	118.38(1)	118.37(4)
V (Å^3)	220.97(1)	226.40(3)
ρ_{calc} (g cm^{-3})	5.485	5.635
2θ range (°)	10–153	10–135
λ (Å)	1.8855	1.6653
No. of reflns	159	204
No. of variables	28	27
$R_P/R_{wP}/R_B$	7.3/8.8/4.6%	4.5/5.7/2.9%

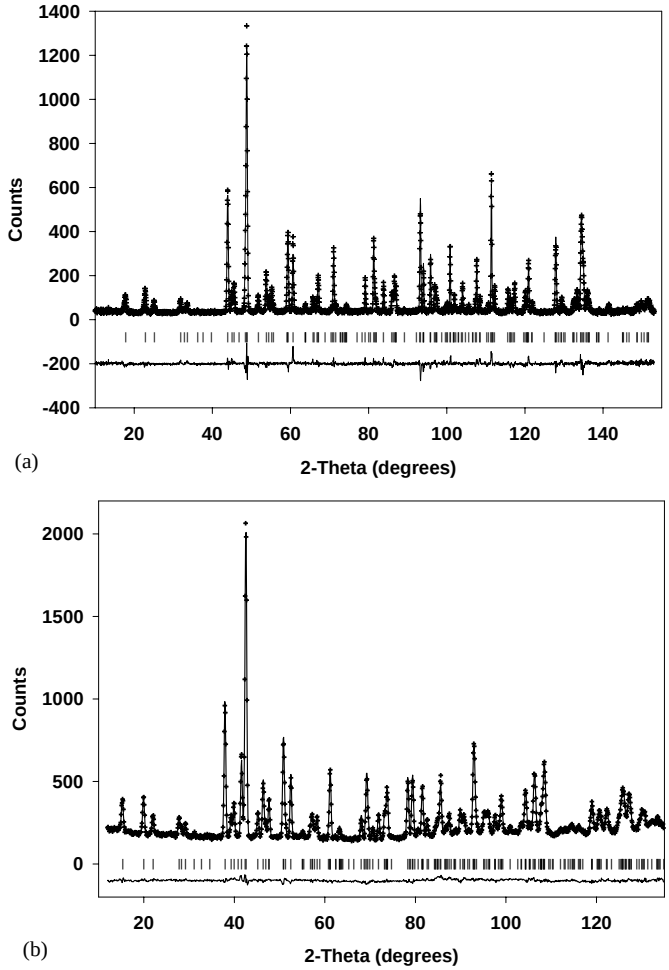

FIG. 2. The observed (crosses), calculated and difference (solid lines) powder neutron diffraction profiles for (a) $U_{0.74}Ca_{0.26}Ti_2O_6$ (**1**) and (b) $U_{0.55}La_{0.45}Ti_2O_6$ (**2**).

the refined atomic positions and thermal parameters are given in Table 4 and the refined structure (of **1**) is displayed in Fig. 3. Selected bond lengths and angles are displayed in Tables 5 and 6, respectively.

As has been observed in numerous perovskite-based compounds, significant variation in ionic size or charge can lead to ordering of the individual ionic species onto distinct crystallographic sites along with an accompanying change in unit cell dimensions (i.e., the formation of a super-lattice structure). Careful examination of the neutron and X-ray diffraction profiles did not provide any evidence for cation ordering in these phases, despite the substantial charge and ionic radii difference between Ca^{2+} and U^{5+} and the very large difference in ionic radii ($\sim$35%) between U^{5+} and La^{3+}.

The structure of $U_{1-x}M_xTiO_6$ consists of sheets of corner and edge-sharing TiO_6 octahedra in the *ab* plane (Fig. 3). The U/*M* atoms adopt an irregular 8-fold

TABLE 4

Fractional Atomic Coordinates and Equivalent Isotropic Thermal Parameters (B_{eq}) ($Å^2 \times 100$) for $U_{0.74}Ca_{0.26}Ti_2O_6$ (1) and $U_{0.55}La_{0.45}Ti_2O_6$ (2) with E.s.d.'s in Parentheses

		1	2
M^a	B_{eq}	0.7(1)	1.1(1)
	Occ	0.26	0.45
U^a	B_{eq}	0.7(1)	1.1(1)
	Occ	0.74	0.55
Ti^b	x	0.8255(5)	0.8270(8)
	z	0.3927(6)	0.3964(12)
	B_{eq}	0.7(1)	0.6(1)
$O1^b$	x	0.9787(3)	0.9791(4)
	z	0.3059(4)	0.3131(8)
	B_{eq}	0.8(1)	1.1(1)
$O2^b$	x	0.6518(3)	0.6563(5)
	z	0.1066(4)	0.1106(9)
	B_{eq}	1.1(1)	1.4(1)
$O3^b$	x	0.2856(2)	0.2858(5)
	z	0.4111(4)	0.4109(6)
	B_{eq}	0.9(1)	1.4(1)

[a]Located at *2a* (0,0,0) site.
[b]Located at *4i* (x,0,z) sites.

coordination between these sheets. The average Ti–O bond lengths in **1** (1.957 Å) and **2** (1.956 Å) are slightly shorter than those typically observed by Shannon (2.005 Å) for other oxides of Ti(IV) (14). In addition, within each TiO_6 octahedron there is significant variation of Ti–O bond lengths (Table 5) and O–Ti–O angles (Table 6), reflecting an irregular coordination. Where octahedra share a

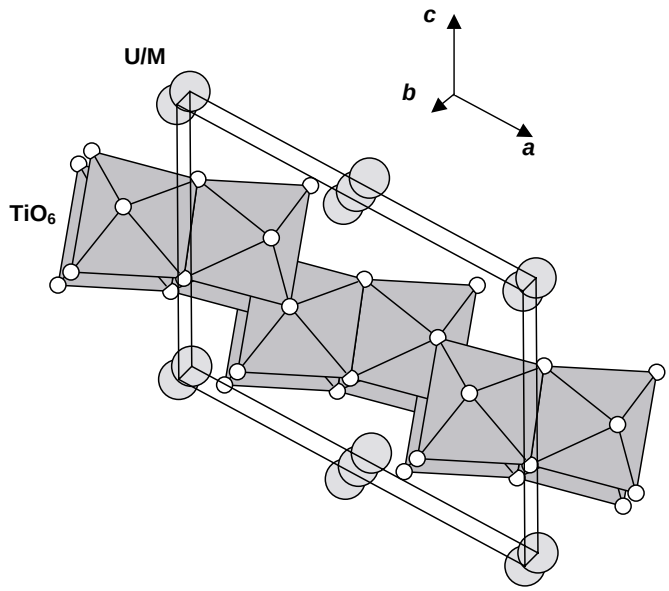

FIG. 3. The refined crystal structure of $U_{0.74}Ca_{0.26}Ti_2O_6$ (**1**), showing sheets of corner and edge-sharing TiO_6 octahedra along the *ab* plane and 8-fold coordinate U/Ca atoms between the planes.

TABLE 5
Selected Bond Lengths (Å) for $U_{0.74}Ca_{0.26}Ti_2O_6$ (1) and $U_{0.55}La_{0.45}Ti_2O_6$ (2) with E.s.d.'s in Parentheses

	1	2
M/U–O1 (×2)	2.210(2)	2.296(6)
M/U–O2 (×4)	2.278(2)	2.309(3)
M/U–O3 (×2)	2.881(3)	2.909(3)
Ti–O1	1.860(4)	1.841(11)
Ti–O1	2.049(5)	2.018(7)
Ti–O2	1.893(4)	1.903(8)
Ti–O3	2.098(5)	2.111(12)
Ti–O3 (×2)	1.921(1)	1.931(3)

common edge, the average distance between adjacent oxygen atoms is 2.50 Å, while the average distance between corner-sharing oxygen atoms is substantially longer at 2.85 Å. The average observed U/*M*–O bond lengths for **1** and **2** (2.412 and 2.456 Å, respectively) are both slightly longer than expected for other uranium containing oxides (2.36 and 2.41 Å, respectively) (14). An examination of Table 5 and Fig. 3 reveals three distinct types of U/*M*–O bonds: a pair of short U/*M*–O1 bonds; four short bonds to O2 atoms that bridge pairs of U/*M* atoms along the *b*-axis and a pair of long U/*M*–O3 bonds.

Bond Valence Sums

The valence of a site (i) may be calculated by the following expression:

$$V_i = \sum_j \exp((r_0 - r_{ij})/B),$$

TABLE 6
Selected Bond Angles (°) for $U_{0.74}Ca_{0.26}Ti_2O_6$ (1) and $U_{0.55}La_{0.45}Ti_2O_6$ (2)

O1–*M*/U–O2	92.1(1)	91.5(2)
O1–*M*/U–O3	63.5(1)	62.4(2)
O2–*M*/U–O2	70.2(1)	71.3(2)
O2–*M*/U–O3	60.2(1)	59.7(2)
O1–Ti–O1	79.3(1)	78.6(3)
O1–Ti–O2	97.6(1)	96.1(4)
O1–Ti–O2	176.8(1)	174.7(5)
O1–Ti–O3	82.7(1)	83.4(4)
O1–Ti–O3	93.2(1)	93.9(3)
O1–Ti–O3	104.0(1)	103.7(2)
O1–Ti–O3	161.9(1)	162.0(4)
O2–Ti–O3	87.6(1)	87.4(2)
O2–Ti–O3	100.5(1)	101.9(4)
O3–Ti–O3	76.9(1)	77.3(2)
O3–Ti–O3	152.0(1)	152.4(4)

where r_{ij} are the observed bond lengths (Table 6), $B = 0.37$ and values of r_0 are those of Brown and Altermatt (15), with the exception of that for U^{5+}–O (2.094 Å) which we determined as the average of those for U^{4+}–O and U^{6+}–O. Bond valence values were calculated based on the quantities of *M*, U^{4+} and U^{5+} as listed in Table 3, giving 3.9(1) and 4.0(1) for the Ca^{2+}/U and La^{3+}/U sites, respectively.

CONCLUSIONS

We have synthesized the doped uranium brannerite phases ($U_{1-x}M_xTi_2O_6$; $M = Ca^{2+}$, La^{3+} and Gd^{3+}) and found the solid solution range to vary depending on the atmosphere used and the charge of the dopant. Each of the phases produced was found to form a monoclinic structure. Rietveld refinement of powder neutron diffraction data of $U_{0.74}Ca_{0.26}Ti_2O_6$ (**1**) and $U_{0.55}La_{0.45}Ti_2O_6$ (**2**) confirms that doping of lower valence M atoms into these brannerite phases occurs in conjunction with the oxidation of U(IV) to U(V).

REFERENCES

1. J. T. Szymanski and J. D. Scott, *Canad. Mineral.* **20,** 271–279 (1982).
2. J. E. Patchett and E. W. Nuffield, *Canad. Mineral.* **6,** 483–490 (1960).
3. A. E. Ringwood, S. E. Kesson, N. G. Ware, W. Hibberson, and A. Major, *Nature (London)* **278,** 219–223 (1979).
4. B. B. Ebbinghaus, R. A. VanKonynenburg, F. J. Ryerson, E. R. Vance, M. W. A. Stewart, A. Jostsons, J. S. Allender, T. Rankin, and J. Congdon, "Ceramic Formulation for the Immobilization of Plutonium," Waste Management '98 (CD-ROM), Tucson, AZ, USA, March 5, 1998.
5. E. R. Vance, M. W. A. Stewart, R. A. Day, K. P. Hart, M. J. Hambley, and A. Brownscombe, "Pyrochlore-rich Titanate ceramics for Incorporation of Plutonium, Uranium and Process Chemicals," ANSTO Report, 1997.
6. Y. Zhang, K. P. Hart, W. L. Bourcier, R. A. Day, M. Colella, B. Thomas, Z. Aly, and A. Jostsons, *J. Nucl. Mater.* **289,** 245–262 (2001).
7. E. R. Vance, J. N. Watson, M. L. Carter, R. A. Day and B. D. Begg, *J. Am. Ceram. Soc.* **84,** 141–144 (2001).
8. A. E. Ringwood, S. E. Kesson, K. D. Reeve, D. M. Levins, and E. J. Ramm, *in* "Radioactive Waste Forms for the Future" (W. Lutze and R. C. Ewing, Eds.), "Synroc;" pp. 223–334. Elsevier, Amsterdam, Netherlands, 1988.
9. S. J. Kennedy, *Adv. X-ray Anal.* **38,** 35–46 (1995).
10. H. M. Rietveld, *J. Appl. Crystallogr.* **2,** 65–71 (1969).
11. B. A. Hunter, "Rietica — A Visual Rietveld Program," *in* "Commission on Powder Diffraction Newsletter," Vol. 20, p. 21 (1998). Available at: http://www.iucr.org/iucr-top/comm/cpd/Newsletters/
12. W. A. Dollase, *J. Appl. Crystallogr.* **19,** 267–272 (1986).
13. A. Le Bail, H. Duroy, and J. L. Fourquet, *Mat. Res. Bull.* **23,** 447–452 (1988).
14. R. D. Shannon, *Acta Crystallogr. A* **32,** 751–767 (1976).
15. I. D. Brown and D. Altermatt, *Acta Crystallogr. B* **41,** 244–247 (1985).